Neurobiology of Disease

GABA Transporter Deficiency Causes Tremor, Ataxia, Nervousness, and Increased GABA-Induced Tonic Conductance in Cerebellum

Chi-Sung Chiu,[1,6] Stephen Brickley,[2] Kimmo Jensen,[3,4] Amber Southwell,[1] Sheri Mckinney,[1] Stuart Cull-Candy,[5] Istvan Mody,[3] and Henry A. Lester[1]

[1]Division of Biology, California Institute of Technology, Pasadena, California 91125, [2]Biophysics Section, Imperial College London, London SW7 2AZ, United Kingdom, [3]Departments of Neurology and Physiology, School of Medicine, University of California Los Angeles, Los Angeles, California 90095-1769, [4]Department of Physiology, University of Aarhus, DK-8000 Aarhus C, Denmark, [5]Department of Pharmacology, University College London, London WC1E 6BT, United Kingdom, and [6]Department of Neurobiology, Merck Research Laboratories, West Point, Pennsylvania 19486

GABA transporter subtype 1 (GAT1) knock-out (KO) mice display normal reproduction and life span but have reduced body weight (female, −10%; male, −20%) and higher body temperature fluctuations in the 0.2–1.5/h frequency range. Mouse GAT1 (mGAT1) KO mice exhibit motor disorders, including gait abnormality, constant 25–32 Hz tremor, which is aggravated by flunitrazepam, reduced rotarod performance, and reduced locomotor activity in the home cage. Open-field tests show delayed exploratory activity, reduced rearing, and reduced visits to the central area, with no change in the total distance traveled. The mGAT1 KO mice display no difference in acoustic startle response but exhibit a deficiency in prepulse inhibition. These open-field and prepulse inhibition results suggest that the mGAT1 KO mice display mild anxiety or nervousness. The compromised GABA uptake in mGAT1 KO mice results in an increased $GABA_A$ receptor-mediated tonic conductance in both cerebellar granule and Purkinje cells. The reduced rate of GABA clearance from the synaptic cleft is probably responsible for the slower decay of spontaneous IPSCs in cerebellar granule cells. There is little or no compensatory change in other proteins or structures related to GABA transmission in the mGAT1 KO mice, including GAT1-independent GABA uptake, number of GABAergic interneurons, and $GABA_A$-, vesicular GABA transporter-, GAD65-, and GAT3-immunoreactive structures in cerebellum or hippocampus. Therefore, the excessive extracellular GABA present in mGAT1 KO mice results in behaviors that partially phenocopy the clinical side effects of tiagabine, suggesting that these side effects are inherent to a therapeutic strategy that targets the widely expressed GAT1 transporter system.

Key words: **tiagabine; epilepsy; flunitrazepam; cerebellum; inhibition; tremor**

Introduction

GABA is the principal inhibitory neurotransmitter in the mammalian brain, where it activates $GABA_A$, $GABA_B$, and $GABA_C$ receptors. GABA released from presynaptic terminals is removed from the vicinity of the synaptic cleft by GABA transporters, and this action is believed to be a key event in terminating synaptic currents. GABA transporters are also involved in maintaining a low extracellular GABA concentration throughout the brain, preventing excessive tonic activation of synaptic and extrasynaptic receptors. GABA transporters may also play a role in replenishing the supply of presynaptic transmitter. Furthermore, GABA transporters may reverse, under both normal and pathological circumstances, to release GABA (Richerson and Wu, 2003, 2004).

Of the three GABA transporters identified in the CNS, GABA transporter subtype 1 (GAT1) is highly expressed in the olfactory bulb, neocortex, cerebellum, superior colliculus, and substantia nigra, where it is predominantly found in axons, presynaptic terminals, and glial cells. GAT2 is weakly expressed throughout the brain, primarily in arachnoid and ependymal cells. GAT3 expression is densest in the olfactory bulb, midbrain regions, and deep cerebellar nuclei, where it is found predominantly on glial cells (Radian et al., 1990; Ikegaki et al., 1994; Itouji et al., 1996; Yan et al., 1997; Engel and Wu, 1998; Barakat and Bordey, 2002; Chiu et al., 2002).

The GAT1 inhibitor tiagabine is a clinically useful antiepileptic drug with few cognitive side effects (Aldenkamp et al., 2003), but it also causes tremor (its major side effect), ataxia, dizziness, asthenia, somnolence (sedation), and nonspecific nervousness (Adkins and Noble, 1998; Pellock, 2001; Schachter, 2001). It is important to know whether these side effects arise directly from increased extracellular concentration of GABA in the CNS or, instead, from actions on unintended targets. For instance, GAT1

Received Aug. 16, 2004; revised Jan. 25, 2005; accepted Jan. 25, 2005.

This research was supported by National Institutes of Health Grants DA-01921, NS-11756, MH-49176, NS-030549, and DA-010509, National Science Foundation Grant 0119493, the Wellcome Trust, a Royal Society-Wolfson Award (S.C.-C.), and a Della Martin Fellowship (C.-S.C.). We are indebted to members of Caltech and University of California Los Angeles groups for advice, Limin Shi and Paul Patterson for use and help with the startle system, and J. Crawley for comments on this manuscript.

Correspondence should be addressed to Henry A. Lester, Division of Biology, California Institute of Technology, 156-29, 1201 East California Boulevard, Pasadena, CA 91125. E-mail: lester@caltech.edu.

DOI:10.1523/JNEUROSCI.3364-04.2005

 0270-6474/05/253234-12$15.00/0

inhibitors may also inhibit $GABA_A$ receptors (Overstreet et al., 2000; Jensen et al., 2003). If the latter mechanism holds, then a more selective GAT1 inhibitor could be a more effective antiepileptic.

To address this question, we examined the phenotype of the ultimate GAT1-specific inhibitor: genetic interruption of GAT1 function. The homozygous and heterozygous mouse GAT1 (mGAT1) knock-out (KO) strain is viable and fertile, with a normal life span. Its hippocampal electrophysiology has been studied previously (Jensen et al., 2003), but this is the first report of several other phenotypes, including motor behavior, general mood, cerebellar electrophysiology, and thermoregulation. We emphasize measurements on the cerebellum, where GAT1 is heavily expressed and has been quantified (Chiu et al., 2002).

GABA influences circadian rhythm (Liu and Reppert, 2000). Because tiagabine-treated patients show dizziness, asthenia, and somnolence, we determined whether the GAT1 KO mice display altered activity in their habituated home cage. We also monitored body temperature rhythm, which is synchronized with daily activity (Weinert and Waterhouse, 1999). We found that the mGAT1 KO mouse does phenocopy some effects of tiagabine, which, in turn, suggests that the various clinical side effects of this drug result, directly or indirectly, from its blockade of GAT1. We measure altered synaptic physiology, deriving from increased and prolonged extracellular [GABA], which provides a plausible physiological basis for these effects.

Materials and Methods

GAT1 knock-out strain. The mGAT1 KO strain, previously termed "intron-14-neo-mGAT1," carries an intact neomycin selection marker in intron 14. The details of the targeting construct, homologous recombination, and genotyping were described previously (Chiu et al., 2002).

Synaptosomal GABA uptake assay. Details of synaptosomal preparation and GABA uptake assay were described previously (Chiu et al., 2002). Briefly, mice were anesthetized with halothane (2-bromo-2-chloro-1,1,1-trifluorothane), and brains were dissected and collected on ice. The cerebellum (~50 mg) was homogenized in 20× (w/v) medium I (0.32 M sucrose, 0.1 mM EDTA, and 5 mM HEPES, pH 7.5; 1 ml) (Nagy and Delgado-Escueta, 1984). The P2 fraction (synaptosome fraction) was suspended with 1 ml of medium I. Protein concentrations were analyzed by using the Coomassie Plus kit (Pierce, Rockford, IL).

GABA uptake assays were performed by mixing 20 μl of the suspension with 280 μl of uptake buffer (in mM: 128 NaCl, 2.4 KCl, 3.2 $CaCl_2$, 1.2 $MgSO_4$, 1.2 KH_2PO_4, 10 glucose, 25 HEPES, pH 7.5) and then incubated at 37°C for 10 min (Lu et al., 1998). GABA and [^{3}H]GABA in various concentrations (100 μl) were added to the synaptosome suspension and incubated for 10 min (final radioactive concentrations were 2.2–8.8 μCi/ml). Uptake was terminated by placing the samples in an ice-cold bath, followed by two washes with uptake buffer containing the same concentration of cold GABA at 10,000 × *g*. The GABA uptake inhibitor 1-[2-[[(diphenylmethylene)imino]oxy]ethyl]-1,2,5,6-tetrahydro-3-pyridinecarboxylic acid hydrochloride (NO711) (final concentration, 30 μM) was included to measure the non-GAT1 uptake activity; the NO711-sensitive fraction accounted for 75–85% of wild-type (WT) activity.

Tremor measurements. The mouse was placed in a 2 L polyethylene freezer container. A piezoelectric transducer (LDT0–028K; Measurement Specialties, Fairfield, NJ) was taped to the bottom of a 7.5 × 10 cm plastic board (8 g), and this board was loosely attached to the bottom of the container with a loop of paper tape. The mice were placed directly on the board. The signal from the sensor was low-pass filtered at 200 Hz, amplified by 100 (model 902; Frequency Devices, Haverhill, MA), and led to the analog-to-digital inputs on an Axon DigiData 1200 interface (Axon Instruments, Union City, CA). The signals were collected using Clampex Gap-Free recording, and power spectra were computed in ClampFit. We verified that the resonant frequency of this instrument was far from the tremor frequency by replacing the mouse with 20 g of mass, and the response of the instrument to constant-frequency mechanical stimulation varied, with frequency, by <40% between 20 and 32 Hz.

Benzodiazepine modulation of the tremor. Mice were tested for baseline tremor as described previously. They were then injected intraperitoneally with either flunitrazepam in 20% FreAmine HBC (B Braun Medical, Bethlehem, PA) or vehicle. After 15 min, the tremor was measured.

Footprint. Hindpaws were painted with black India ink, and mice were placed in a cardboard box (90 × 12 × 12 cm) with a 75-cm-long white paper floor. Paw angle is the hindpaw central axis relative to its walking direction.

Rotarod. Mice were tested on a motorized rotarod (Ugo Basile, Comerio, Italy) consisting of a grooved metal roller (3 cm in diameter) and separated 11-cm-wide compartments elevated 16 cm. The acceleration rate was set at 0.15 rpm/s. Mice were placed on the roller, and the time they remained on it during rotation was measured. The rotarod has an increment of 4 rpm/step. Tests were performed for fixed speed at either 12 or 20 rpm and for accelerating speed. A maximum of 120 s was allowed per animal for fixed speed tests.

Exploratory locomotor activity. An individual mouse was placed in a novel environment of a square open field (50 × 50 cm), the floor of which was divided into 25 smaller squares (5 × 5) by painted lines. Within 10 cm of the chamber walls is termed the periphery (16 squares), and the central region indicates the central nine squares. The animal behavior in the open field was recorded by videotaping for 10 min and analyzed subsequently. The measurements include delayed exploratory activity (measuring the time required for mice to walk the first 50 cm), frequency of visits to the central area, dwell time in the inner field, number of rearing events, total distance traveled, and walking speed. Mice usually made short walks interrupted by brief stops. To make meaningful walking-speed measurements, we chose uninterrupted walking for >25 cm and averaged 3–12 such walking-speed measurements for each animal. All animals were tested in a particular behavioral assay on the same day during the light part of the light/dark cycle.

Elevated plus maze. Mice were allowed to habituate to the testing room for 2 h. The maze consisted of two opposing open arms (40 × 10 cm) and two opposing closed arms (40 × 10 cm, with 40 cm walls) on a platform 50 cm above the ground. Mice were placed in the center square (10 × 10 cm) facing an open arm and videotaped during a 5 min exploration. Arm entries and duration were scored when all four paws entered the arm. Partial arm entries were scored when one to three paws entered the arm. Head dipping was scored when the head was dipped over the edge of the maze. All animals were tested on the same day during the light part of the light/dark cycle.

Home-cage activity. Mice were housed individually in cages with bedding, food, and water. To assess activity, beam breaks were collected for 42 h with a photo beam system (San Diego Instruments, San Diego, CA). Plots show the number of beam breaks for each 5 min interval.

Benzodiazepine hyperlocomotor activity. Mice were allowed to habituate to activity cages for 2 h. They were then injected intraperitoneally with either flunitrazepam in 20% FreAmine HBC (5 or 15 mg/kg) or vehicle. Activity (single beam breaks) and ambulation (successive beam breaks) data were then collected for 1 h and plotted for each 5 min interval.

Acoustic startle and prepulse inhibition. Animals were tested in a Startle Response system (SR-LAB; San Diego Instruments) consisting of a 5 cm Plexiglas cylinder mounted on a Plexiglas platform in a ventilated, lighted, sound-attenuated chamber. Acoustic stimuli were presented by a high-frequency loudspeaker mounted 28 cm above the cylinder. A piezoelectric accelerometer attached to the Plexiglas base was used to detect movement of the animals within the cylinder. Animal movement was scored in arbitrary numbers between 0 and 1000. Ambient background noise of 68 dB was maintained throughout each testing session. Each session was initiated with a 5 min acclimation period followed by six 120 dB trials and concluded with another six 120 dB trials. These first and last sets of six 120 dB pulses were not included in the analysis. For acoustic startle-response (ASR) testing, seven different levels of acoustic startle pulse (73, 78, 83, 85, 100, 110, and 120 dB) were presented along with a trial containing only the background noise for 40 ms each in random

order with variable intertrial intervals of 10–20 s. At the onset of stimulus, 65 startle-amplitude readings were taken for 1 ms each. Ten trials of each decibel level were performed, and the average startle amplitude was determined. The session used for prepulse inhibition (PPI) testing consisted of five different trials presented 10 times each in random order. These include 120 dB startle pulse alone, 120 dB startle pulse preceded by a prepulse of 73, 78, or 83 dB (5, 10, and 15 dB above background), and a trial containing only the background noise. The percentage of prepulse inhibition was calculated as follows: 100 × [(average 120 dB startle pulse − average prepulse + 120 dB startle pulse)/average 120 dB startle pulse].

Temperature measurements. Mini Mitter (Sunriver, OR) ER-4000 telemetric temperature probes were used in 3- to 6-month-old male mGAT1 KO mice. For implantation, mice were anesthetized with halothane, and a 1 cm incision was made at the back of the neck. Probes were inserted subcutaneously into the back. The incision was sealed with surgical glue. The mice were housed with *ad libitum* water and food at 24 ± 2.5°C. Lights were on between 6:00 A.M. and 6:00 P.M. for 7–10 d after implantations and then off for the period of data collection. Temperature and activity data were acquired using Vital View software (Mini-Mitter) and analyzed (including fast Fourier transforms) in Origin.

Seizure tests. Pentylenetetrazole (PTZ) was solubilized in 0.9% NaCl saline solution, and bicuculline was dissolved in 0.1N HCl, pH adjusted to 5.5 with 0.1N NaOH (Pericic and Bujas, 1997). Animals were injected intraperitoneally with either PTZ or bicuculline. For PTZ, animals were injected with either subthreshold (40 mg/kg) or suprathreshold (70 mg/kg) doses. For bicuculline, animals were injected with 3, 4, or 5 mg/kg.

Brain slice electrophysiology. Cerebellar slices were prepared using standard procedures (Brickley et al., 1996). The brain was rapidly dissected and submerged in cold slicing solution (~4°C), which contained the following (in mM): 125 NaCl, 2.5 KCl, 1 $CaCl_2$, 4 $MgCl_2$, 25 $NaHCO_3$, 1.25 NaH_2PO_4, and 25 glucose. All extracellular solutions were bubbled with 95% O_2 and 5% CO_2, pH 7.4. After cutting on a moving-blade microtome, slices were maintained at 32°C for 60 min before transfer to a recording chamber. For granule cell recordings, slices were constantly perfused (1.5 ml/min) with recording solution containing the following (in mM): 125 NaCl, 2.5 KCl, 2 $CaCl_2$, 1 $MgCl_2$, 26 $NaHCO_3$, 1.25 NaH_2PO_4, and 25 glucose. For Purkinje cell recordings, slices were perfused with the following (in mM): 126 NaCl, 2.5 KCl, 2 $CaCl_2$, 2 $MgCl_2$, 26 $NaHCO_3$, 1.25 NaH_2PO_4, 10 glucose, 0.2 L-ascorbic acid, 1 pyruvic acid, and 3 kynurenic acid. All experiments were performed at room temperature, and whole-cell voltage-clamp recordings were made using Axopatch 1D or 200B amplifiers (Axon Instruments). The pipette solution contained the following (in mM): 140 CsCl, 4 NaCl, 0.5 $CaCl_2$, 10 HEPES, 5 EGTA, 2 Mg-ATP, adjusted to pH 7.3 with CsOH.

Currents were filtered at 2–3 kHz and digitized at 10 kHz. The tonic $GABA_A$ receptor-mediated conductance (G_{GABA}) was measured from the reduction in holding current recorded in the presence of the $GABA_A$ receptor antagonist 2-(3-carboxypropyl)-3-amino-6-(4-methoxyphenyl)-pyridazinium bromide (SR95531) (>100 μM). All-points histograms were constructed from sections of data not containing synaptic currents and mean values calculated from a Gaussian fit to the histogram. Spontaneous IPSCs (sIPSCs) were detected with amplitude- and kinetics-based criteria (events were accepted when they exceeded a threshold of 6–8 pA for 0.5 ms) using custom-written LabView-5.1-based software (National Instruments, Austin, TX). All IPSCs were also inspected visually, and sweeps were rejected or accepted manually. Individual spontaneously occurring IPSCs were then aligned on their initial rising phase, and average IPSC waveforms were constructed from those events that exhibited a clear monotonic rise and returned to baseline before the occurrence of later sIPSCs. The decay of average

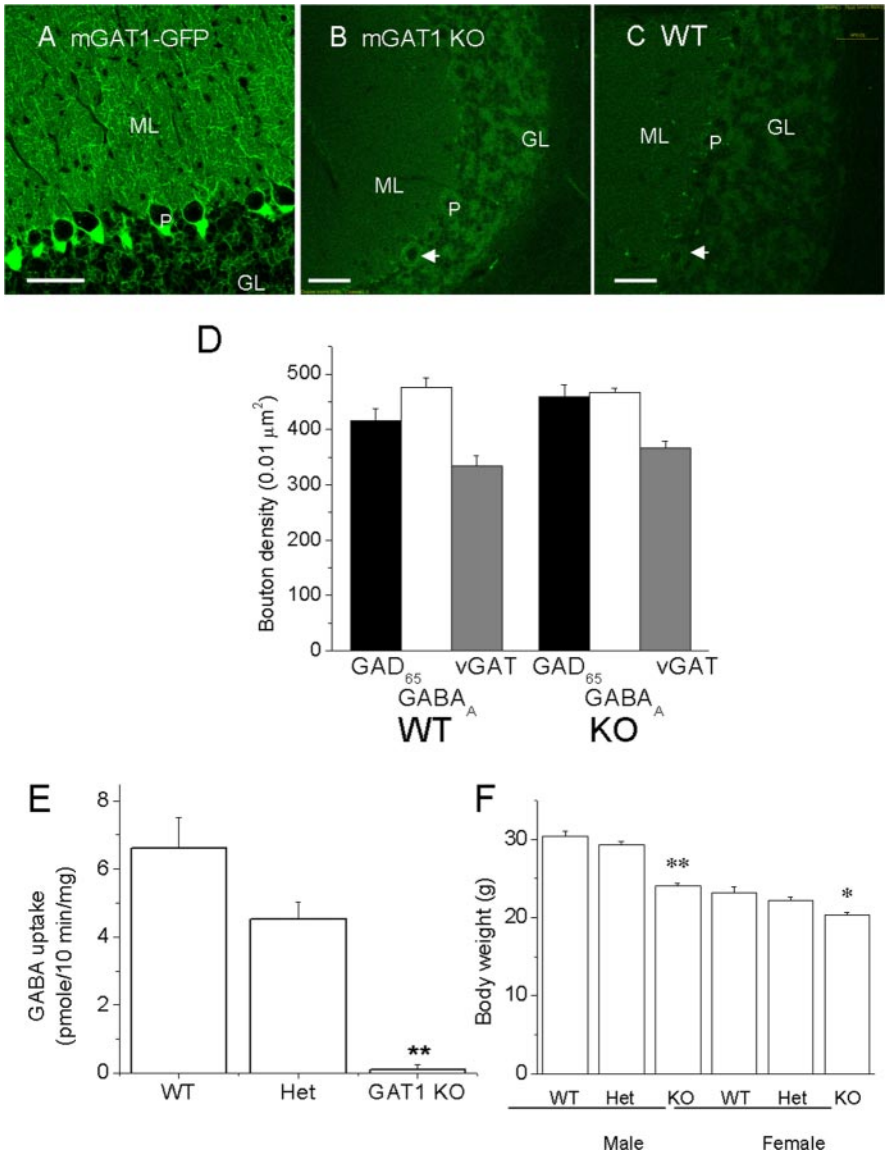

Figure 1. mGAT1 KO cerebellar images, synaptosomal GABA uptake, and body weight. ***A***, Fluorescent image of an mGAT1-GFP knock-in mouse cerebellar cortex, showing typical GAT1 expression pattern. ***B***, Fluorescent image of GAT1 KO showing no obvious GAT1 expression pattern. ***C***, WT mouse shows no obvious fluorescence. ***B*** and ***C*** were exposed to >20-fold greater photo power than ***A***. GL, Granule cell layer; ML, molecular layer; P, Purkinje cell. Scale bar, 50 μm. ***D***, Quantification of GAD65, vGAT, and $GABA_A$ receptor-containing boutons in WT and KO mice based on the immunocytochemical staining (see supplemental figure for the actual images, available at www.jneurosci.org as supplemental material). ***E***, The NO711-sensitive synaptosomal [^{3}H]GABA uptake activities among the three genotypes (mean ± SEM; triplicate assays from each of two experiments with all three genotypes). ***E***, Decreased body weight of the GAT1 KO mouse. Data measured from 11 litters of het/het matings between the ages of 50 and 66 d are shown. Compared with WT littermates, male homozygotes weigh ~20% less, whereas female homozygotes weigh ~10% less. M, Male; F, female. WT, Het, KO: $n = 8, 17, 15$ for males; $n = 11, 14, 8$ for females. Differences from WT at $^*p < 0.05$ and $^{**}p < 0.01$.

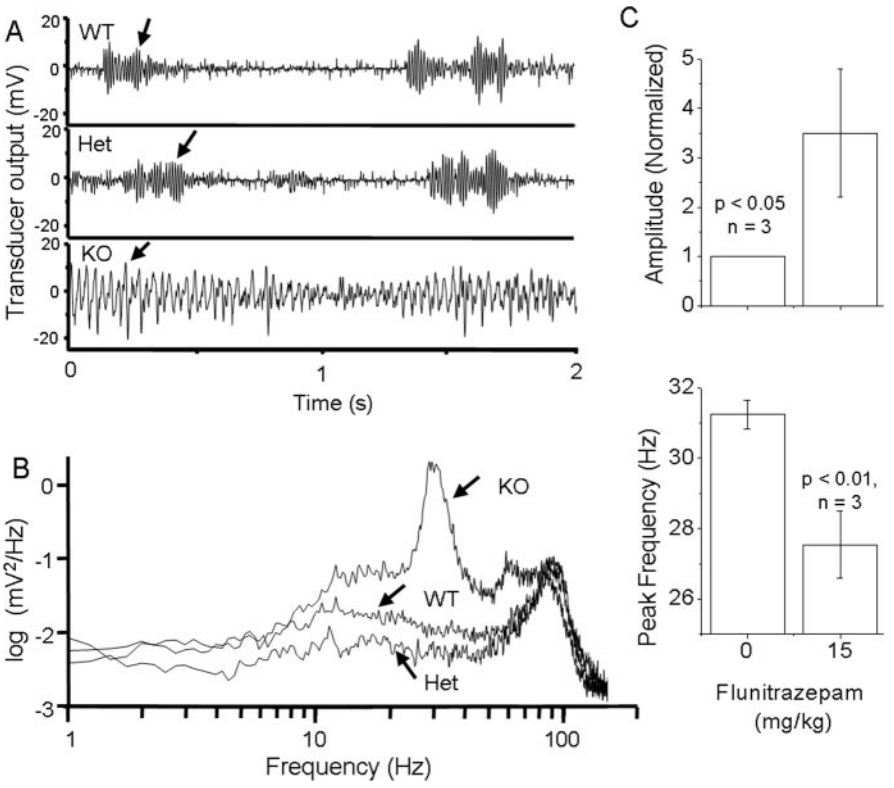

Figure 2. Characterization of mGAT1 KO tremor. ***A***, Recordings from the vibration transducer. Arrows (higher amplitude) indicate activities when forepaws were raised. ***B***, Power spectrum of the transducer signal for all genotypes. All genotypes shared a minor peak at ~80 Hz; however, only the KO showed a significant tremor at 25–32 Hz. ***C***, Modulation of tremor frequency and amplitude by flunitrazepam. Error bars represent SEM.

sIPSC waveforms was quantified as a weighted τ value calculated from the charge transfer of normalized averages ($\tau_{integral}$).

Immunocytochemistry. Detailed procedures for immunocytochemistry were described previously (Chiu et al., 2002; Jensen et al., 2003). Mice were anesthetized with halothane and perfused with 4% paraformaldehyde in PBS, pH adjusted to 7.6 with Na_2HPO_4. Brains were dissected and kept in 4% paraformaldehyde for 1 h in 4°C and then incubated in 30% sucrose in PBS for ~20 h. The brains were embedded in OCT medium (Tissue-Tek; Miles, Elkhart, IN) for either horizontal or sagittal sections and sliced by cryostat at 35 μm. Brain slices were stored in a solution containing the following (in mM): 11 NaH_2PO_4, 20 Na_2HPO_4, 30% ethylene glycol, and 30% glycerol, pH 7.5, at −20°C.

Sections were incubated for 2 h at room temperature in a blocking solution (10% normal goat serum and 0.3% Triton X-100 in PBS, pH 7.6), followed by incubation with the primary antibody for 2 d at 4°C with rotational mixing. Primary antibodies and their dilutions were rabbit anti-GAT3 (1:200 dilution; Chemicon, Temecula, CA), rabbit anti-$GABA_A$ receptor α1 (1:100; Upstate Biotechnology, Lake Placid, NY), rabbit anti-glutamate decarboxylase 65 (GAD65) (1:1000; Chemicon), and rabbit anti-vesicular GABA transporter (vGAT) (1:100; Synaptic Systems, Goettingen, Germany). The brain slices were first washed with PBS containing 0.5% Triton X-100 followed by two additional washes with PBS. The slices were then incubated in solutions containing the appropriate rhodamine red-x-conjugated secondary antibodies. These secondary antibodies include goat anti-rabbit, goat anti-guinea pig, or donkey anti-goat secondary antibodies (1:200; Jackson ImmunoResearch, West Grove, PA). After three washes with PBS, slices were rinsed with PBS, mounted with Vectashield (Vector Laboratories, Burlingame, CA), and subjected to confocal microscope imaging.

Results

Evidence for functional knock-out of GAT1

The knock-in mouse strain studied here, previously termed intron-14-neo-intact-mGAT1, harbors a neomycin resistance cassette (*neo*) in intron 14 as well as a green fluorescent protein (GFP) moiety fused to the C terminus of the mGAT1 coding region in exon 14 (Jensen et al., 2003). This strain was originally constructed as a genetic intermediate in the eventual construction of a *neo*-deleted mGAT1-GFP knock-in strain that has also been described previously (Chiu et al., 2002). However, we found that the present strain appears to have essentially no functional mGAT1 (Jensen et al., 2003), presumably because the *neo* sequences interfere with mRNA or protein. Figure 1 shows additional evidence on this point in the cerebellum, for which we later provide electrophysiological data. First, the GFP moiety at the C terminus of the GAT1 construct provides a fluorescent label for the level of GAT1 expression (Chiu et al., 2002). The mGAT1 KO strain shows <2% as much fluorescence as the mGAT1-GFP strain (Chiu et al., 2002) and no more fluorescence than WT mice (Fig. 1*A–C*). Second, to measure mGAT1 function, we performed GABA uptake assays on cerebellar synaptosomes. The NO711-sensitive GABA uptake activity from mutant mice synaptosomes was <2% of that of WT littermates, whereas heterozygotes displayed intermediate GABA uptake activity (Fig. 1*E*), indicating that mutant mice have little or no functional presynaptic GAT1 activity. mGAT1-deficient mice also display reduced body weight, ~20 and ~10% less than WT for males and females, respectively (Fig. 1*F*).

Cerebellar immunocytochemistry

To test whether the mGAT1 KO mouse has abnormalities in the GABAergic system, we performed immunocytochemistry on several proteins related to GABA function. Immunocytochemistry using antibodies against GAD65, the $GABA_A$ α1 subunit and the vGAT indicated that mGAT1 KO mice do not change GABAergic synapse densities and related receptor expression in the molecular layer of the cerebellum (summarized in Fig. 1*D*) (based on images in the supplemental figure, available at www.jneurosci.org as supplemental material). We also found no qualitative differences in $GABA_A$ α1 subunit staining in the granule cell layer (data not shown). These data agree with previous data on the hippocampus (Jensen et al., 2003). Also, the expression pattern for GAT3 is not changed, suggesting that no compensatory changes occurred because of the GAT1 deficit (see supplemental figure, available at www.jneurosci.org as supplemental material). Immunocytochemistry using antibodies against GABAergic, interneuron-specific, calcium-binding proteins showed no changes in GABAergic interneuron density in the hippocampus and in the cerebellum.

Behavioral characterizations of GAT1 KO mice

Tremor

The mGAT1 KO mice display readily observable, nearly continuous tremor in the limbs and tail. Measured by a simple instrument (Fig. 2*A*) (see Materials and Methods), the tremor fre-

quency is 25–32 Hz (Fig. 2*B*). In addition, KO and WT share an additional lower amplitude tremor at ~80 Hz (Fig. 2*B*) ($n = 6$). Vibrations in both frequency ranges are highest during rearing episodes (Fig. 2*A*, arrows). Acute high-dose NO711 treatment caused complete sedation in WT mice, vitiating any observations on tremor in NO711-treated WT mice.

Flunitrazepam treatment decreased the frequency and increased the amplitude of the tremor in mGAT1 KO mice (Fig. 2*C*) but had very little effect on the power spectrum of WT mice (data not shown). These effects in KO mice were both significant for 15 mg/kg flunitrazepam; both effects were intermediate for 10 mg/kg flunitrazepam, but only the frequency change was significant for 10 mg/kg flunitrazepam.

Ataxia

Ataxia is associated with cerebellar defects in many strains of mice (Mullen et al., 1976; Watanabe et al., 1998; Rico et al., 2002). The mGAT1 KO mice walk with an abnormally large paw angle relative to the direction of walking: 23 ± 0.7 versus 12.5 ± 1.4° for KO and WT, respectively (Fig. 3*E*,*F*). In another indication of ataxia, mGAT1 KO mice display flattened stance and lowered hip on the rotarod (Fig. 3*B*). The mGAT1 KO mice show reduced time on the rotarod in both fixed speed (Fig. 3*C*) and accelerating speed (Fig. 3*D*) tests, indicating ataxia. Both WT and mutant mice improved performance on the rotarod after training; however, the difference of latency to fall remained significant between WT and KO mice (data not shown). The mGAT1 KO and WT mice displayed equal muscle strength in hanging-wire activity tests (data not shown).

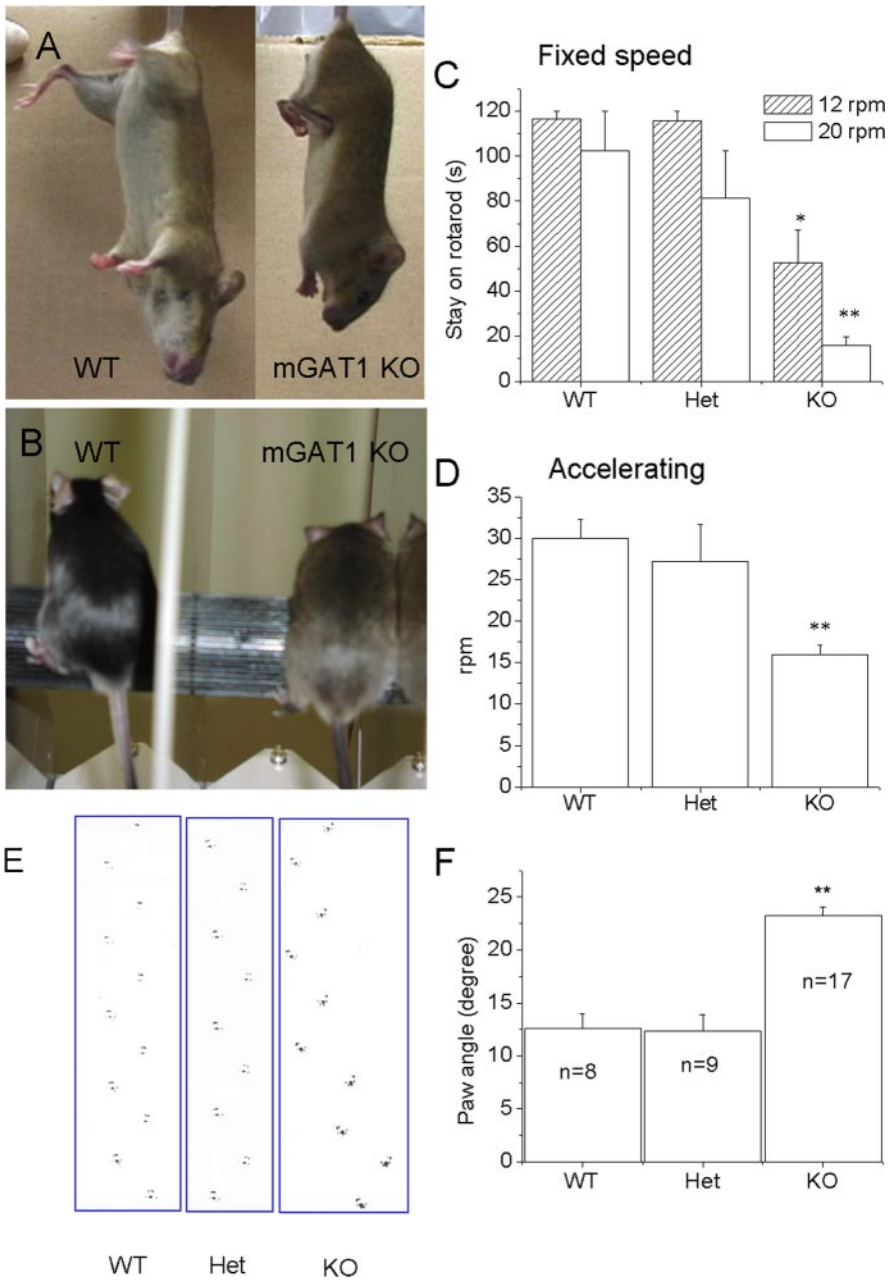

Figure 3. mGAT1 KO displays abnormal motor behavior. ***A***, WT (left) and mGAT1 KO (right) mice showed different gestures when hung by their tails. WT mice showed a typical extensor gesture, whereas KO mice showed flexor contraction. ***B***, Stance of WT and KO mice on the rotarod. The KO mice show flattened and lowered hips, and their paws move more slowly than WT mice. ***C***, Mice were tested at fixed speed (either 12 or 20 rpm) on the rotarod. $n = 6$, 5, and 8 (WT, Het, and KO, respectively). ***D***, Mice were tested at accelerating speeds. KO mice fell significantly sooner than WT mice. ***E***, Abnormal gait. Hindpaw footprint pattern of WT, heterozygotes, and homozygotes is shown. The hindpaws of mGAT1 KO mice show a wider angle with respect to the direction of walking. The KO mouse seems to waddle. ***F***, Comparison of the average paw angles among WT ($n = 8$), Het ($n = 9$), and KO ($n = 17$) mice. The paw angle of the KO mouse is approximately twice as large as that of WT and heterozygotes (23 ± 1 vs 12.5 ± 1°). Differences from WT at $^*p < 0.05$ and $^{**}p < 0.01$.

Mild anxiety: flexor contraction, exploratory activity, elevated plus maze, and startle

When suspended by the tail, the mGAT1-deficient mice display trembling and flexor contraction (front paws held together and rear paws flexed) (Fig. 3*A*). This gesture resembles typical mouse models for anxiety. WT littermates displayed normal extension without trembling (Fig. 3*A*). The flexor contraction was also observed in WT mice treated with a high dose of NO711 (10–40 mg/kg; data not shown).

The open field was used as an additional test of anxiety-like behavior (Fig. 4) (Prut and Belzung, 2003). Because an open field is a novel environment, rodents tend to prefer the periphery of the apparatus, later exploring the central parts of the open field. We observed several aspects of behavior in this apparatus. The mGAT1 KO mice tend to remain longer in the corner of the open field (Fig. 4*A*) and then tend to walk slowly along the wall; thus, there was markedly reduced frequency of visits to the central area (Fig. 4*B*), reduced dwell time in the central area (Fig. 4*C*), and reduced rearing activity (Fig. 4*D*). These results may signify anxiety of the mGAT1 KO mice. There was modestly reduced walking speed (Fig. 4*E*). Although WT and heterozygotes walk faster than KO mice, they spend more time in rearing; as a consequence, all three genotypes traveled about the same distance (Fig. 4*F*). Several of the observations in the open-field test suggest that the

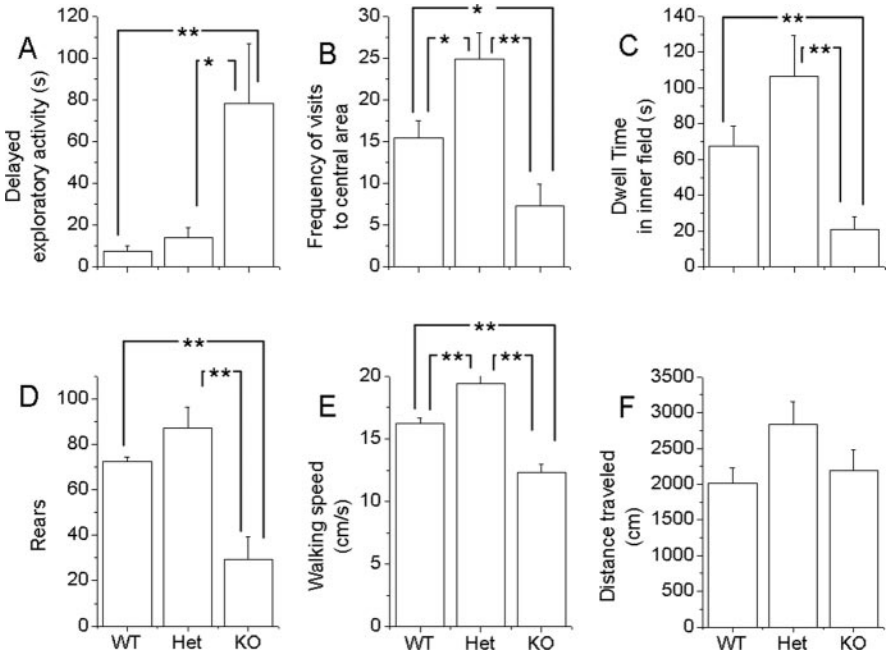

Figure 4. Characterization of mGAT1 KO exploratory activity in the open field. ***A***, The time required for mice to walk the first 50 cm in open field. Most WT and Het mice take <10 s, whereas KO mice spend 13–240 s. Points show mean ± SEM. ***B***, ***C***, The KO mouse shows reduced frequency (***B***) and reduced duration (***C***) visiting the central area in the open-field test. Total visits to the central area were 15 ± 2, 25 ± 3, and 7 ± 3, and total time to stay in the central area were 67 ± 11, 106 ± 23, and 21 ± 7 s for WT, Het, and KO, respectively. ***D***, The GAT1 KO mouse showed reduced frequencies of rearing (73 ± 2, 87 ± 9, and 29 ± 10 for WT, Het, and KO, respectively). ***E***, The average walking speeds for WT, Het, and KO mice were 16.2 ± 0.5, 19.4 ± 0.6, and 12.3 ± 0.6 cm/s, respectively. ***F***, mGAT1 KO mice showed no obvious difference in total walking distance within 10 min (2000 ± 210, 2840 ± 320, and 2190 ± 300 for WT, Het, and KO, respectively). ***E***, $n = 7$, 12, and 10 (WT, Het, and KO, respectively). For all other panels, $n = 6$, 8, and 8 (WT, Het, and KO, respectively). *$p < 0.05$; **$p < 0.01$.

heterozygote is the least anxious phenotype; we did not explore this observation systemically.

We observed the mGAT1 KO mice in the elevated plus maze, another test of anxiety (Fig. 5*A*,*B*). The mGAT1 KO mice displayed increased partial arm entries (Fig. 5*A*) and time spent in the central square (Fig. 5*B*) compared with WT mice. Homozygous mutant mice showed reduced open-arm entries and reduced total time spent in the open arms (data not shown). There was a trend toward reduced closed-arm entries; however, this difference was not statistically significant compared with WT. Mutant mice spent the majority of the testing time in the central square engaging in partial-arm entries, indicating no reduction in locomotor activity. No difference was seen in head dipping. Thus, the elevated plus maze provided some additional evidence for anxiety.

Startle is a fast twitch of facial and body muscles evoked by sudden and intense tactile, visual, or acoustic stimulations. Many anxious mouse strains display both enhanced ASR and reduced PPI. The mGAT1-deficient mice display normal ASR (Fig. 5*C*) but reduced PPI (Fig. 5*D*), compared with their WT littermates. The baseline movement of the mGAT1 mutant in the absence of acoustic stimulation was elevated above the WT. This most likely reflects the constant tremor of these mice.

Ambulation activity

The mGAT1 KO mice show reduced ambulation in their cages; as a consequence, the 24 h activity cycle becomes less obvious (Fig. 6*A*). The total ambulation activities were 2425 ± 395 versus 965 ± 146 times during 42 h for WT and mGAT1 KO mice, respectively (Fig. 6*B*) (mean ± SEM). Flunitrazepam treatment caused hyperlocomotor activity in KO animals and sedation in WT animals (data not shown).

Autonomic regulation: body temperature fluctuations

The mGAT1 KO mice display a striking pattern of abnormal temperature regulation (Fig. 7*A*,*B*). There is a normal circadian temperature rhythm, but in addition, there are many fluctuations, primarily hyperthermic episodes on a time scale of several minutes to ~2 h. To quantify these fluctuations, we computed and averaged the power spectral density of temperature fluctuations in WT or KO mice (Fig. 7*C*). The data have been normalized to the peak at 0.0416 h^{-1} (corresponding to the circadian rhythm). It is clear that mGAT1 KO mice display increased relative noise power in the frequency range from 0.2 to 1.5 h^{-1}. The mGAT1 hyperthermic episodes are larger, especially during high activity (i.e., higher body temperature), but no more frequent than in WT mice (Fig. 7*B*). Two additional animals in each group provided similar data, but these animals were not included in the averaged power spectra because of differences in sample rate.

Sensitivity to convulsants

The mGAT1 KO mouse is slightly more sensitive than the WT mouse to PTZ-induced seizures, but there is no obvious change in bicuculline-induced seizure susceptibility. Bicuculline (i.p.) at 5 mg/kg kills WT and mGAT1 KO mice, whereas at 3 and 4 mg/kg, both WT and KO mice survived with moderate seizure ($n = 2$ each). PTZ at a subthreshold dose (40 mg/kg, i.p.) decreased observable activity in WT and heterozygotes while causing preconvulsive states and mild seizures in mGAT1 KO mice ($n = 3$ each). At a suprathreshold dose (70 mg/kg), all WT and heterozygotes survived with severe seizures, whereas mGAT1 KO mice showed severe seizures, and one of three died ($n = 3$ each).

Cerebellar slice electrophysiology

$GABA_A$ receptor-mediated currents, recorded from wild-type mice, are similar to those reported previously (Brickley et al., 2001) (Fig. 8). Granule cells dialyzed with high-internal Cl^- and voltage clamped at −70 mV (see Materials and Methods) exhibit sIPSCs, with a frequency of 0.8 ± 0.6 Hz ($n = 4$). In addition, a tonic $GABA_A$ receptor-mediated conductance (G_{GABA}) is clearly present in all recordings. The phasic and tonic conductances are both blocked by the $GABA_A$ receptor antagonist SR95531 (>100 μM) (Fig. 8*A*). The magnitude of G_{GABA} (84.2 ± 50.4 pS/pF) is similar to previous reports for animals of this age, as are the peak amplitude (388.5 ± 143.3 pS/pF) and kinetics ($\tau_{integral}$ = 17.6 ± 3.3 ms) of average sIPSCs (Brickley et al., 2001).

Recordings from mGAT1 KO cerebellar granule cells reveal marked differences in both the tonic and phasic conductances, consistent with the removal of a GABA transporter. In all seven recordings from mGAT1 KO mice, G_{GABA} is significantly increased (Fig. 8*B*) to an average value of 318.9 ± 65.6 pS/pF ($p <$

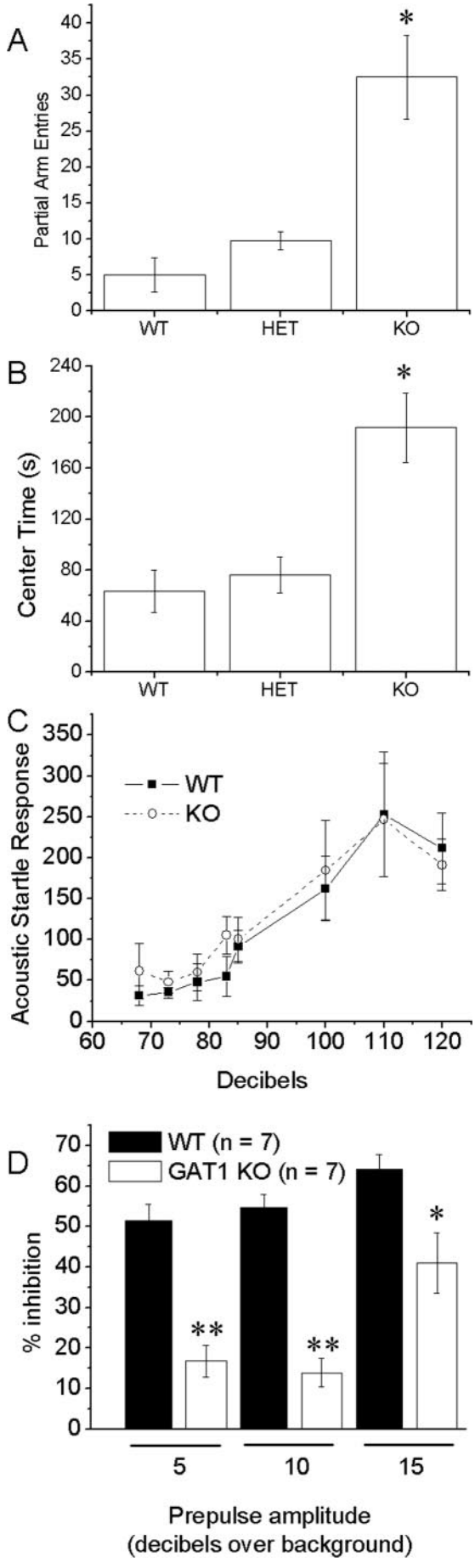

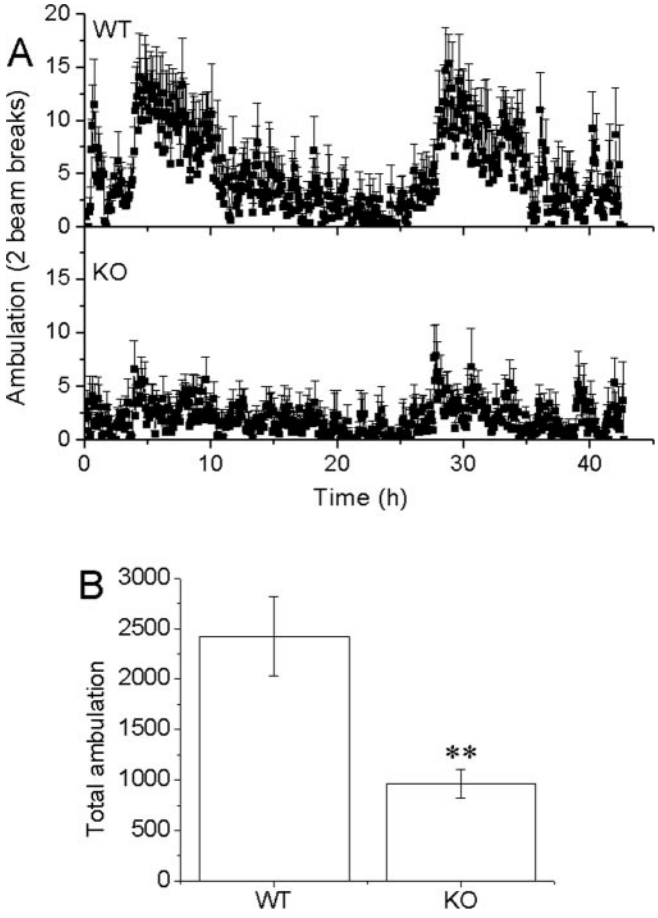

Figure 6. GAT1 KO mice showed reduced ambulation in home cages. ***A***, Profiles of ambulation activity of WT (top) and KO (bottom) mice over a 42 h recording period. WT displays a 24 h rhythm, whereas KO shows lower activity. ***B***, Total ambulation activity of KO and WT mice (2425 ± 395 and 965 ± 146 counts). Error bars represent SEM.

0.05) (Fig. 8*C*). Conventional sIPSCs (Fig. 8*D*,*E*) are still detectable within the current record, albeit at an apparently lower average frequency (0.4 ± 0.2 Hz). The increased current variance associated with G_{GABA} (Fig. 8*E*, histogram) made resolution of small sIPSCs more difficult. Nevertheless, it appears that the average peak amplitude is not significantly different in the mGAT1 KO recordings (270.5 ± 31.5 pS/pF). However, as shown in Figure 8*F*, the decay of sIPSCs is slower in the mGAT1 KO cells ($\tau_{integral}$ = 36.9 ± 5.7 ms compared with 17.6 ± 3.3 ms in wild-type granule cells). Therefore, in mature cerebellar granule cells, we observed an ~300% increase in the magnitude of G_{GABA} and a 100% increase in the decay time of sIPSCs after the removal of GAT1.

In Purkinje cell recordings, a standing inward $GABA_A$ receptor-mediated conductance, defined by sensitivity to the $GABA_A$ receptor antagonist SR95531 (>100 μM), was observed

←

Figure 5. Additional anxiety-related behaviors: elevated plus maze and acoustic startle. mGAT1 KO mice display increased partial arm entries (***A***) and time spent in the central square (***B***) compared with WT mice. *$p < 0.01$; $n = 4$ mice in each group. ***C***, Acoustic startle response of mutant (open circle; $n = 4$) and WT (filled square; $n = 4$) measured in arbitrary units. ***D***, Prepulse inhibition of mutant (open column; $n = 7$) and WT (filled column; $n = 7$). The 5, 10, and 15 under the *x*-axis refer to prepulses at 5, 10, and 15 dB, respectively, above the background level of 68 dB. The difference between KO and WT is significant at *$p < 0.05$ and **$p <$ 0.01. Error bars represent SEM.

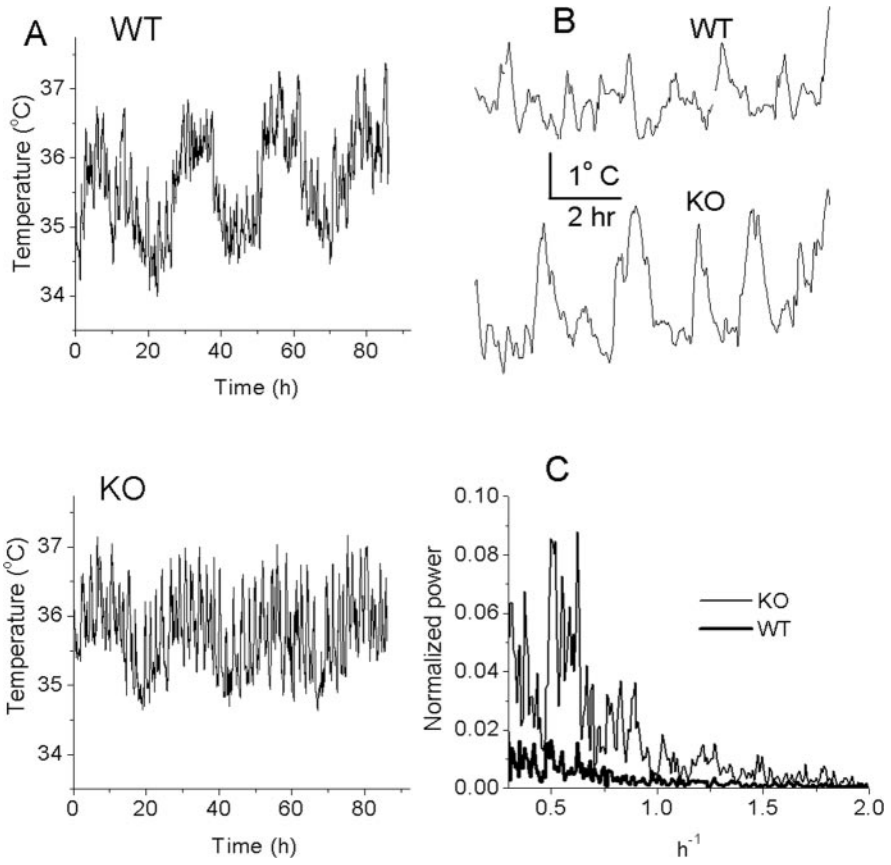

Figure 7. mGAT1-deficient mice display more body temperature fluctuations in the 0.2–1.5/h frequency range than WT mice. ***A***, Raw traces of body temperature fluctuation from one WT (top) and one mutant (bottom) mouse. Mutant mice display multiple hyperthermic episodes, especially during periods of higher activity (i.e., higher body temperature). ***B***, Expanded traces from ***A***. ***C***, Power spectrum analysis. The *y*-axis represents the average power ($n = 4$ KO, 3 WT) normalized to the peak at 24 h cycle as 100%. The *x*-axis represents the frequency (inverse hours).

in mGAT1 KO mice, which is much larger than in WT mice (75 ± 19 pS/pF, $n = 10$ vs 13 ± 5 pS/pF, $n = 9$, respectively) (Fig. 9). However, the high frequency of sIPSCs consistently observed in Purkinje cells (>10 Hz) indicates that a comparison of sIPSC kinetics between WT and mGAT KO mice is not possible in this cell type because of the considerable superimposition of events. Moreover, it is not feasible to selectively analyze the tonic and phasic components of the $GABA_A$-mediated conductance in a similar manner to the granule cell recordings. Nonetheless, as shown in Figure 9, it is clear that in Purkinje cell recordings, the magnitude of a standing inward $GABA_A$ receptor-mediated conductance is significantly increased in mGAT1 KO mice.

Discussion

The mGAT1 KO mouse as a model for tiagabine side effects

The distinct phenotype of mGAT1 KO mice includes ataxia, tremor, sedation, nervousness (mild anxiety), increased frequency and amplitude of body temperature fluctuations, and reduced body weight. Similar behavioral patterns were also observed in WT mice treated with either tiagabine or NO711, both GAT1 inhibitors (Nielsen et al., 1991; Suzdak et al., 1992; Suzdak, 1994). Epileptic patients treated with Tiagabine display similar side effects, including dizziness, asthenia, somnolence (sedation), nonspecific nervousness, tremor, and ataxia (Adkins and Noble, 1998). The fact that the mGAT1 KO mice phenocopy many effects of both mice and humans treated with GAT1 inhibitors suggests that the clinical side effects might be expected from any systemically administered drug that targets GAT1, no matter how selective.

Synaptic basis of the tremor

GAT1 inhibition causes elevated extracellular [GABA] and therefore generates an increased tonic $GABA_A$-mediated conductance, perhaps primarily by acting at areas that typically express high-affinity, nondesensitizing $GABA_A$ receptors (Brickley et al., 1996; Wall and Usowicz, 1997; Hamann et al., 2002; Jensen et al., 2003). Our data for cerebellar granule (Fig. 8) and Purkinje (Fig. 9) cells support these ideas. Previous studies also report a prolongation of the evoked $GABA_A$ receptor-mediated synaptic decay after block of GABA transporters (Dingledine and Korn, 1985; Roepstorff and Lambert, 1992, 1994; Thompson and Gahwiler, 1992; Draguhn and Heinemann, 1996; Rossi and Hamann, 1998; Overstreet et al., 2000). This phenomenon is not observed after action potential-independent release (Thompson and Gahwiler, 1992; Isaacson et al., 1993), suggesting that GAT1 transporters are likely to be more important in limiting the GABA profile after multivesicular release. However, the use of GABA transport blockers in previous assays may be complicated by the fact that GAT1 inhibitors are also competitive antagonists of $GABA_A$ receptors (Overstreet et al., 2000; Jensen et al., 2003).

The cerebellar glomerulus, like the basket cell–Purkinje cell pinceau synapse and the chandelier cell–pyramidal cell cartridge of cortex, is a highly organized synaptic structure that contains many synaptic contacts produced by just a few presynaptic inhibitory axons (Jakab and Hamori, 1988) and features a dense level of GAT1 expression (Chiu et al., 2002). The dramatically prolonged granule cell IPSC waveforms in mGAT1 KO mice are certainly consistent with the idea that GAT1 plays a more important role in clearing GABA after multivesicular release in structures such as the glomerulus, where diffusion is limited (Nielsen et al., 2004). This may explain the greater prolongation of sIPSCs we observe in mGAT1 KO granule cells (Fig. 8) than previously observed in hippocampus (Jensen et al., 2003). The unchanged level of GAD65 (Fig. 1*D*), vGAT (Fig. 1*D*), the GABA receptor $\alpha 1$ subunit (Fig. 1*D*), $GABA_B$ receptors (Jensen et al., 2003), and GAT3 (see supplemental figure, available at www.jneurosci.org as supplemental material) in the mGAT1 KO mice argues against some classes of compensatory changes in response to the chronically elevated [GABA]. Furthermore, the NO711-insensitive cerebellar synaptosomal GABA uptake was only 15–25% of the total activity in WT, and the absolute value of NO711-insensitive GABA uptake activity showed no difference between WT and mGAT1 KO. However, we cannot rule out other changes such as altered subunit composition of $GABA_A$ receptors or an altered waveform of synaptically released [GABA]. Whatever the underlying synaptic mechanisms, the distorted inhibitory waveform observed in granule cells suggests that inhibition in one or more motor control nuclei provides a reasonable, although not quan-

titative, explanation for the tremor that we observed in the mGAT1 KO mouse. An oscillation between excitation and inhibition underlies many neuronal pacemakers, and in mGAT KO mice, this oscillation is apparently timed in part by the accentuated inhibitory phase that results from increased and prolonged [GABA]. Flunitrazepam, an allosteric activator of $GABA_A$ receptors, increased the period and increased the amplitude of the tremor (Fig. 2*C*), consistent with the idea that one phase of the oscillation is governed by the waveform of $GABA_A$-mediated inhibition.

Which inhibitory synapse(s) dominates the tremor? We do not imply that the oscillation is solely determined by the timing of a cerebellar inhibitory synapse such as the Golgi cell–granule cell contact. The removal of GAT1 presumably alters characteristics of GABA-mediated transmission in many nuclei. $GABA_A$ receptor α1 subunit knock-out mice tremble at ~18 Hz (Kralic et al., 2002), suggesting that a tremor can arise from either too little or too much GABAergic transmission throughout the brain. However, the tremor in mGAT1 KO mice is inconsistent with the low-frequency tremors generally associated with basal ganglia and midbrain pathology. The tremor also has a higher frequency (25–32 Hz) (Fig. 2) than most previously reported mouse tremors but equal to that of mice expressing the hypofunctional glycine receptor (GlyR) *oscillator* α1 subunit (Simon, 1997) or a human hyperekplexia-related GlyR mutant (Becker et al., 2002). Glycine transporter 2 knock-out mice also display 15–25 Hz tremor (Gomeza et al., 2003). These observations on the glycinergic system suggest that the tremor is primarily spinal in origin.

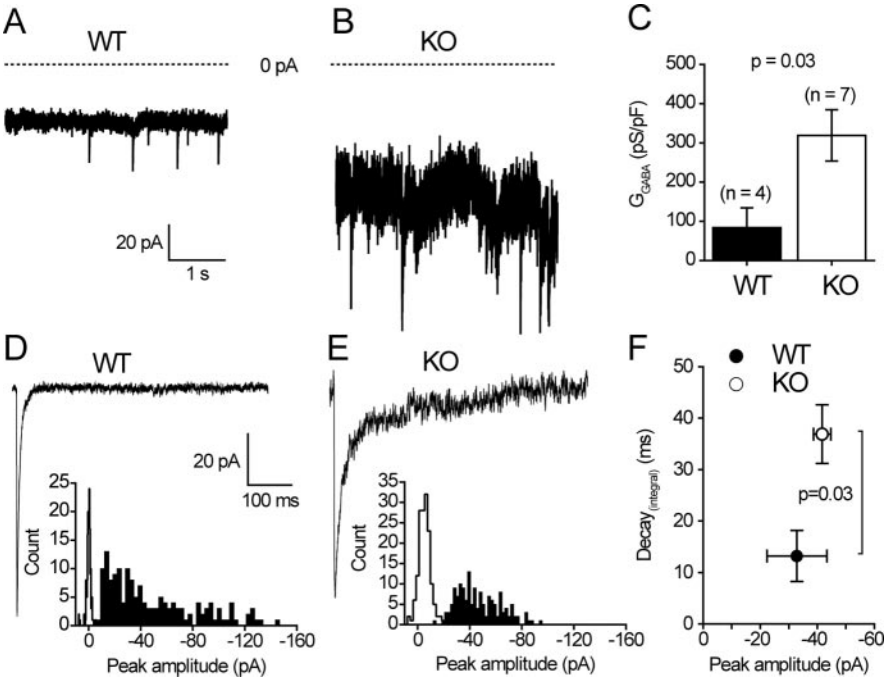

Figure 8. mGAT1 KO cerebellar granule cells are characterized by an increased tonic $GABA_A$-mediated conductance and prolonged IPSCs. ***A***, ***B***, Continuous current records from typical wild-type (***A***) and mGAT1 KO (***B***) internal granule cells voltage clamped at −70 mV. The horizontal line indicates the 0 current level in each recording. There is an increased inward current in mGAT1 KO cells and a substantial increase in the current variance associated with this conductance. This increased tonic conductance is completely blocked by the $GABA_A$ receptor antagonist SR95531 (gabazine). ***C***, The bar graph illustrates that, on average, G_{GABA} in GAT1 KO granule cells was 319 ± 65 pS/pF ($n = 7$) compared with 84 ± 50 pS/pF ($n = 4$) in control littermates. This resembles the 98 ± 20 pS/pF G_{GABA} recorded previously in the C57BL/6 strain (Brickley et al., 2001). Therefore, the tonic conductance tripled after the removal of GAT1, indicating a raised concentration of ambient GABA in the slice preparation. ***D***, ***E***, Two average sIPSC waveforms recorded from a wild-type (***D***) and an mGAT1 KO (***E***) granule cell are shown on the same scale. The waveforms have similar peak amplitudes but very different decays. The histograms also illustrate the peak amplitude distribution of all sIPSCs recorded in these cells. The open histograms were constructed from periods of baseline noise. As shown by the increase in the width of the baseline histogram for mGAT1 KO, the increased current variance associated with mGAT1 KO recordings does complicate interpretation of peak amplitude measurements. It is possible that we are missing a significant fraction of small events in the mGAT1 KO, because they would be unresolved in the noisy mGAT1 KO recordings. However, this possible artifact does not affect the decay estimates, because the decay of sIPSCs is not correlated with peak amplitude in granule cells (data not shown). ***F***, The significant increase in the decay of sIPSC recorded from mGAT1 KO granule cells. The decay was defined as $\tau_{integral}$ (see Materials and Methods). The $\tau_{integral}$ of control littermates was 13 ± 5 ms ($n = 4$) compared with 37 ± 6 ms ($n = 5$) in the mGAT1 KO animals. In contrast, there was no significant difference between the average peak amplitudes recorded in the two strains. Error bars represent SEM.

Ataxia

The ataxia exhibited by mGAT1-deficient mice (i.e., rotarod deficits) (Fig. 3*C*,*D*; broader paw angle in *E*,*F*) is more likely to originate from a specific cerebellar defect, because ablation of GABAergic neurons in the cerebellum also causes ataxia in several classic mouse mutants. Overall, these results illustrate that normal motor control depends on maintaining appropriate levels of both phasic and tonic $GABA_A$ receptor-mediated inhibition in the cerebellum.

Nervousness versus anxiety

Nervousness describes the clinical side effects of tiagabine (Dodrill et al., 1997, 1998, 2000; Adkins and Noble, 1998). In the absence of an accepted test for nervousness in rodents, we assumed that it can be assessed as a mild form of anxiety. The GAT1 KO mice show such a phenotype. In the open-field test, mGAT1-deficient mice display delayed exploratory activity and decreased frequency of visits to the central area (Fig. 4*A–C*). However, the reduced rearing (Fig. 4*D*) could be caused by simply the decreased motor ability that leads to the lowered stance (Fig. 3*B*); there was only moderately reduced walking speed (Fig. 4*E*) and no reduction in total distance traveled (Fig. 4*F*). Furthermore, mutant mice show no difference in acoustic startle response compared with WT (Fig. 5*C*), but they display a dramatic decrease in prepulse inhibition of the acoustic startle response (Fig. 5*D*). The mGAT1 KO displays reduced home-cage activity, but the modest decrement in open-field walking speed suggests that mutant mice remain active when encountering novel environments, whereas they display reduced activity in a habituated environment (Fig. 5*A*,*B*). In contrast, 5-HT transporter null mice exhibit a classical pattern of increased anxiety-like behavior in the elevated plus maze, in light–dark exploration and emergence tests, and in open-field tests (Holmes et al., 2003).

It is also true that many classical anxiolytic drugs operate by increasing the activity of $GABA_A$ receptors. Likewise, reduced GABA also causes anxiety; for example, GAD65 knock-out mice exhibit increased anxiety-like behavior in both the open-field and elevated-zero maze assays (Kash et al., 1999).

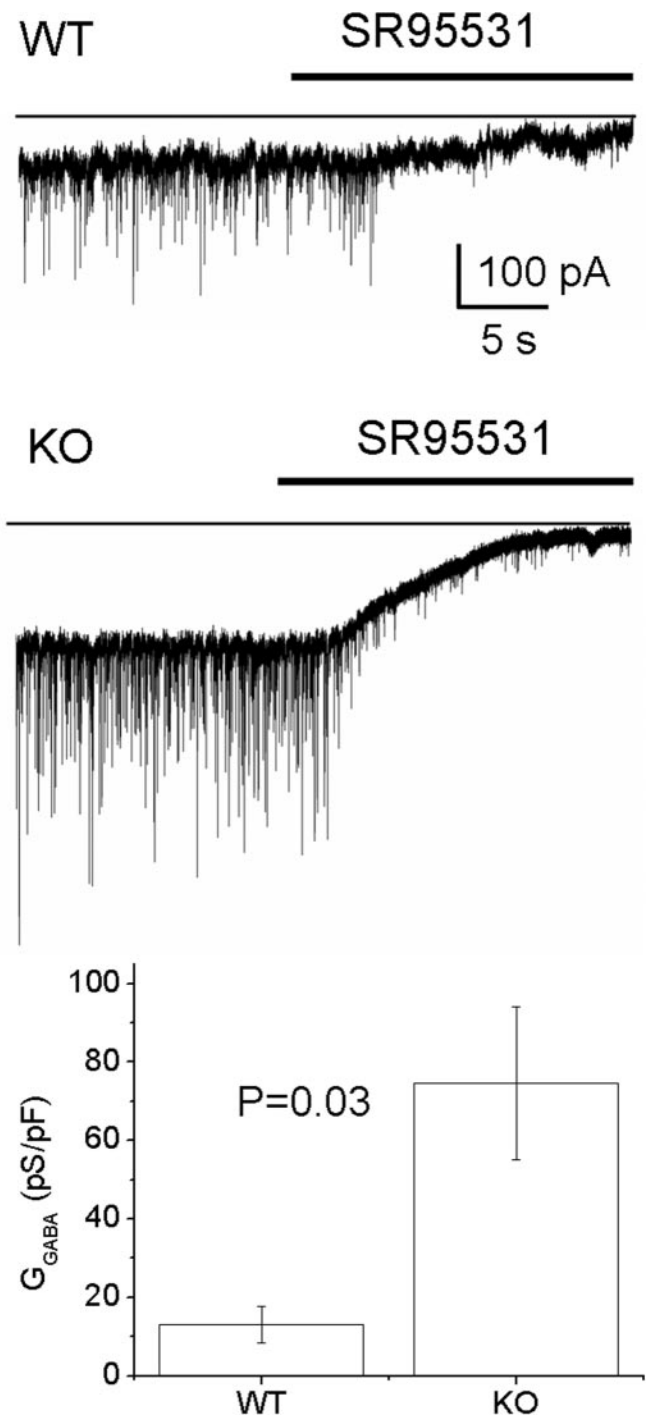

Figure 9. mGAT1 KO mice display higher tonic currents in cerebellar Purkinje cells. In both WT and mGAT1 KO slices, sIPSCs were recorded in Purkinje cells by holding at −70 mV. Zero current levels are shown in the light trace. Injection of SR95531 into the bath (>100 μM; heavy trace) blocked tonic current and sIPSCs. Average tonic currents in mGAT1 KO cells are approximately six times larger than in WT cells [75 ± 19 and 13 ± 5 pS/pF for KO (n = 10) and WT (n = 9), respectively]. Error bars represent SEM.

Reduced body weight

The reduced body weight of mGAT1 KO mice (Fig. 1*F*) contrasts with obesity of transgenic mice overexpressing mGAT1 under nonspecific or pan-neuronal promoters (Ma et al., 2000). GABA-related regulatory mechanism of feeding behavior in the ventromedial hypothalamus may be responsible for impaired responses to glucoprivation in genetically obese rats (Tsujii and Bray, 1991). Benzodiazepine-treated rats lose body weight, presumably via activation of $GABA_A$ receptors (Blasi, 2000). Excess GABA in the anterior piriform cortex region reduces feeding (Truong et al., 2002). We believe that the reduced body weight and tremor is not related to delayed (or retarded) development, because mGAT1 KO mice are reproductive at the same time as WT and display muscle strength and balance similar to WT. Additional detailed studies are required.

Thermoregulation and circadian rhythm

Thermoregulation is controlled by several brain regions, including the horizontal limb of the diagonal band of Broca (HDB), the basal forebrain, the preoptic area (POA), and the rostral part of the raphe pallidus nucleus (rRPa). Many neurons in these areas are GABAergic. In the HDB, muscimol reduces thermosensitivity (Hays et al., 1999) and, in the rRPa, muscimol to rRPa blocks fever and thermogenesis in brown adipose tissue induced by intra-POA as well as by intracerebroventricular prostaglandin E2 applications (Nakamura et al., 2002).

We know of no clinical studies on temperature effects of tiagabine. However, the higher amplitude of hyperthermic episodes in the mGAT1 KO mouse (Fig. 7) clearly does not phenocopy the acute hypothermic effects of tiagabine in rodents (Inglefield et al., 1995). Interestingly, $GABA_B$ activation leads to hypothermia (Schuler et al., 2001), but we found previously that the presynaptic $GABA_B$ response is diminished or lost in mGAT1 KO mice (Jensen et al., 2003), which may explain the discrepancy.

Although GABA has been related to circadian rhythm in many publications (Liu and Reppert, 2000; Wagner et al., 2001), the mGAT1-deficient mice did not display obvious changes in circadian rhythm during 5 d of testing either in constant dark or in a 12 h light/dark cycle environment. These results suggest that excess GABA does not affect circadian rhythm.

An additional use for knock-out mice strains

To the other useful information obtained from knock-out mouse strains, we may add the decision regarding whether the clinical side effects of a drug (in this case, tiagabine) arise from either widespread expression of its target or nonselective actions on other targets. Such information is particularly valuable when the pleiotropic effects cannot readily be predicted from, but are certainly consistent with, the widespread and varied roles of the target molecule. Of course, such a study is rather straightforward when it is believed that the effects are mostly acute and subject to straightforward neurological tests (as in the present case), rather than delayed and primarily psychiatric (as for serotonin and perhaps dopaminergic and noradrenergic transporters).

References

Adkins JC, Noble S (1998) Tiagabine. A review of its pharmacodynamic and pharmacokinetic properties and therapeutic potential in the management of epilepsy. Drugs 55:437–460.

Aldenkamp AP, De Krom M, Reijs R (2003) Newer antiepileptic drugs and cognitive issues. Epilepsia 44 [Suppl 4]:21–29.

Barakat L, Bordey A (2002) GAT-1 and reversible GABA transport in Bergmann glia in slices. J Neurophysiol 88:1407–1419.

Becker L, von Wegerer J, Schenkel J, Zeilhofer HU, Swandulla D, Weiher H (2002) Disease-specific human glycine receptor α1 subunit causes hyperekplexia phenotype and impaired glycine- and $GABA_A$-receptor transmission in transgenic mice. J Neurosci 22:2505–2512.

Blasi C (2000) Influence of benzodiazepines on body weight and food intake

in obese and lean Zucker rats. Prog Neuropsychopharmacol Biol Psychiatry 24:561–577.
Brickley SG, Cull-Candy SG, Farrant M (1996) Development of a tonic form of synaptic inhibition in rat cerebellar granule cells resulting from persistent activation of $GABA_A$ receptors. J Physiol (Lond) 497:753–759.
Brickley SG, Revilla V, Cull-Candy SG, Wisden W, Farrant M (2001) Adaptive regulation of neuronal excitability by a voltage-independent potassium conductance. Nature 409:88–92.
Chiu CS, Jensen K, Sokolova I, Wang D, Li M, Deshpande P, Davidson N, Mody I, Quick MW, Quake SR, Lester HA (2002) Number, density, and surface/cytoplasmic distribution of GABA transporters at presynaptic structures of knock-in mice carrying GABA transporter subtype 1-green fluorescent protein fusions. J Neurosci 22:10251–10266.
Dingledine R, Korn SJ (1985) γ-Aminobutyric acid uptake and the termination of inhibitory synaptic potentials in the rat hippocampal slice. J Physiol (Lond) 366:387–409.
Dodrill CB, Arnett JL, Sommerville KW, Shu V (1997) Cognitive and quality of life effects of differing dosages of tiagabine in epilepsy. Neurology 48:1025–1031.
Dodrill CB, Arnett JL, Shu V, Pixton GC, Lenz GT, Sommerville KW (1998) Effects of tiagabine monotherapy on abilities, adjustment, and mood. Epilepsia 39:33–42.
Dodrill CB, Arnett JL, Deaton R, Lenz GT, Sommerville KW (2000) Tiagabine versus phenytoin and carbamazepine as add-on therapies: effects on abilities, adjustment, and mood. Epilepsy Res 42:123–132.
Draguhn A, Heinemann U (1996) Different mechanisms regulate IPSC kinetics in early postnatal and juvenile hippocampal granule cells. J Neurophysiol 76:3983–3993.
Engel JE, Wu CF (1998) Genetic dissection of functional contributions of specific potassium channel subunits in habituation of an escape circuit in *Drosophila*. J Neurosci 18:2254–2267.
Gomeza J, Ohno K, Hulsmann S, Armsen W, Eulenburg V, Richter DW, Laube B, Betz H (2003) Deletion of the mouse glycine transporter 2 results in a hyperekplexia phenotype and postnatal lethality. Neuron 40:797–806.
Hamann M, Rossi DJ, Attwell D (2002) Tonic and spillover inhibition of granule cells control information flow through cerebellar cortex. Neuron 33:625–633.
Hays TC, Szymusiak R, McGinty D (1999) $GABA_A$ receptor modulation of temperature sensitive neurons in the diagonal band of Broca *in vitro*. Brain Res 845:215–223.
Holmes A, Yang RJ, Lesch KP, Crawley JN, Murphy DL (2003) Mice lacking the serotonin transporter exhibit 5-HT_{1A} receptor-mediated abnormalities in tests for anxiety-like behavior. Neuropsychopharmacology 28:2077–2088.
Ikegaki N, Saito N, Hashima M, Tanaka C (1994) Production of specific antibodies against GABA transporter subtypes (GAT1, GAT2, GAT3) and their application to immunocytochemistry. Brain Res Mol Brain Res 26:47–54.
Inglefield JR, Perry JM, Schwartz RD (1995) Postischemic inhibition of GABA reuptake by tiagabine slows neuronal death in the gerbil hippocampus. Hippocampus 5:460–468.
Isaacson JS, Solis JM, Nicoll RA (1993) Local and diffuse synaptic actions of GABA in the hippocampus. Neuron 10:165–175.
Itouji A, Sakai N, Tanaka C, Saito N (1996) Neuronal and glial localization of two GABA transporters (GAT1 and GAT3) in the rat cerebellum. Brain Res Mol Brain Res 37:309–316.
Jakab RL, Hamori J (1988) Quantitative morphology and synaptology of cerebellar glomeruli in the rat. Anat Embryol (Berl) 179:81–88.
Jensen K, Chiu CS, Sokolova I, Lester HA, Mody I (2003) GABA transporter-1 (GAT1)-deficient mice: differential tonic activation of $GABA_A$ versus $GABA_B$ receptors in the hippocampus. J Neurophysiol 90:2690–2701.
Kash SF, Tecott LH, Hodge C, Baekkeskov S (1999) Increased anxiety and altered responses to anxiolytics in mice deficient in the 65-kDa isoform of glutamic acid decarboxylase. Proc Natl Acad Sci USA 96:1698–1703.
Kralic JE, O'Buckley TK, Khisti RT, Hodge CW, Homanics GE, Morrow AL (2002) Deletion of $GABA_A$ receptor ($GABA_A$-R) α1 subunit alters benzodiazepine (BZD) site pharmacology, function and related behavior. Soc Neurosci Abstr 28:39.12.
Liu C, Reppert SM (2000) GABA synchronizes clock cells within the suprachiasmatic circadian clock. Neuron 25:123–128.
Lu Y, Grady S, Marks MJ, Picciotto M, Changeux JP, Collins AC (1998) Pharmacological characterization of nicotinic receptor-stimulated GABA release from mouse brain synaptosomes. J Pharmacol Exp Ther 287:648–657.
Ma YH, Hu JH, Zhou XG, Zeng RW, Mei ZT, Fei J, Guo LH (2000) Transgenic mice overexpressing gamma-aminobutyric acid transporter subtype I develop obesity. Cell Res 10:303–310.
Mullen RJ, Eicher EM, Sidman RL (1976) Purkinje cell degeneration, a new neurological mutation in the mouse. Proc Natl Acad Sci USA 73:208–212.
Nagy A, Delgado-Escueta AV (1984) Rapid preparation of synaptosomes from mammalian brain using nontoxic isoosmotic gradient material (Percoll). J Neurochem 43:1114–1123.
Nakamura K, Matsumura K, Kaneko T, Kobayashi S, Katoh H, Negishi M (2002) The rostral raphe pallidus nucleus mediates pyrogenic transmission from the preoptic area. J Neurosci 22:4600–4610.
Nielsen EB, Suzdak PD, Andersen KE, Knutsen LJS, Sonnewald U, Braestrup C (1991) Characterization of Tiagabine (NO-328), a new potent and selective GABA uptake inhibitor. Eur J Pharmacol 196:257–266.
Nielsen TA, DiGregorio DA, Silver RA (2004) Modulation of glutamate mobility reveals the mechanism underlying slow-rising AMPAR EPSCs and the diffusion coefficient in the synaptic cleft. Neuron 42:757–771.
Overstreet LS, Jones MV, Westbrook GL (2000) Slow desensitization regulates the availability of synaptic $GABA_A$ receptors. J Neurosci 20:7914–7921.
Pellock JM (2001) Tiagabine (gabitril) experience in children. Epilepsia 42 [Suppl 3]:49–51.
Pericic D, Bujas M (1997) Sex differences in the response to GABA antagonists depend on the route of drug administration. Exp Brain Res 115:187–190.
Prut L, Belzung C (2003) The open field as a paradigm to measure the effects of drugs on anxiety-like behaviors: a review. Eur J Pharmacol 463:3–33.
Radian R, Ottersen OP, Strorm-Mathisen J, Castel M, Kanner BI (1990) Immunocytochemical localization of the GABA transporter in rat brain. J Neurosci 10:1319–1330.
Richerson GB, Wu Y (2003) Dynamic equilibrium of neurotransmitter transporters: not just for reuptake anymore. J Neurophysiol 90:1363–1374.
Richerson GB, Wu Y (2004) Role of the GABA transporter in epilepsy. Adv Exp Med Biol 548:76–91.
Rico B, Xu B, Reichardt LF (2002) TrkB receptor signaling is required for establishment of GABAergic synapses in the cerebellum. Nat Neurosci 5:225–233.
Roepstorff A, Lambert JD (1992) Comparison of the effect of the GABA uptake blockers, tiagabine and nipecotic acid, on inhibitory synaptic efficacy in hippocampal CA1 neurones. Neurosci Lett 146:131–134.
Roepstorff A, Lambert JDC (1994) Factors contributing to the decay of the stimulus-evoked IPSC in rat hippocampal CA1 neurons. J Neurophysiol 72:2911–2926.
Rossi DJ, Hamann M (1998) Spillover-mediated transmission at inhibitory synapses promoted by high affinity α6 subunit $GABA_A$ receptors and glomerular geometry. Neuron 20:783–795.
Schachter SC (2001) Pharmacology and clinical experience with tiagabine. Expert Opin Pharmacother 2:179–187.
Schuler V, Luscher C, Blanchet C, Klix N, Sansig G, Klebs K, Schmutz M, Heid J, Gentry C, Urban L, Fox A, Spooren W, Jaton AL, Vigouret J, Pozza M, Kelly PH, Mosbacher J, Froestl W, Kaslin E, Korn R, et al. (2001) Epilepsy, hyperalgesia, impaired memory, and loss of pre- and postsynaptic $GABA_B$ responses in mice lacking $GABA_{B(1)}$. Neuron 31:47–58.
Simon ES (1997) Phenotypic heterogeneity and disease course in three murine strains with mutations in genes encoding for alpha 1 and beta glycine receptor subunits. Mov Disord 12:221–228.
Suzdak PD (1994) Lack of tolerance to the anticonvulsant effects of tiagabine following chronic (21 day) treatment. Epilepsy Res 19:205–213.
Suzdak PD, Frederiksen K, Andersen KE, Sorensen PO, Knutsen LJ, Nielsen EB (1992) NNC-711, a novel potent and selective gamma-aminobutyric acid uptake inhibitor: pharmacological characterization. Eur J Pharmacol 224:189–198.
Thompson SM, Gahwiler BH (1992) Effects of the GABA uptake inhibitor tiagabine on inhibitory synaptic potentials in rat hippocampal slice cultures. J Neurophysiol 67:1698–1701.

Truong BG, Magrum LJ, Gietzen DW (2002) GABA(A) and GABA(B) receptors in the anterior piriform cortex modulate feeding in rats. Brain Res 924:1–9.

Tsujii S, Bray GA (1991) GABA-related feeding control in genetically obese rats. Brain Res 540:48–54.

Wagner S, Sagiv N, Yarom Y (2001) GABA-induced current and circadian regulation of chloride in neurones of the rat suprachiasmatic nucleus. J Physiol (Lond) 537:853–869.

Wall MJ, Usowicz MM (1997) Development of action potential-dependent and independent spontaneous $GABA_A$ receptor-mediated currents in granule cells of postnatal rat cerebellum. Eur J Neurosci 9:533–548.

Watanabe D, Inokawa H, Hashimoto K, Suzuki N, Kano M, Shigemoto R, Hirano T, Toyama K, Kaneko S, Yokoi M, Moriyoshi K, Suzuki M, Kobayashi K, Nagatsu T, Kreitman RJ, Pastan I, Nakanishi S (1998) Ablation of cerebellar Golgi cells disrupts synaptic integration involving GABA inhibition and NMDA receptor activation in motor coordination. Cell 95:17–27.

Weinert D, Waterhouse J (1999) Daily activity and body temperature rhythms do not change simultaneously with age in laboratory mice. Physiol Behav 66:605–612.

Yan XX, Cariaga WA, Ribak CE (1997) Immunoreactivity for GABA plasma membrane transporter, GAT-1, in the developing rat cerebral cortex: transient presence in the somata of neocortical and hippocampal neurons. Brain Res Dev Brain Res 99:1–19.